

02

*Library Copy
RA A 73462 R.C.*

~~CONFIDENTIAL~~

Copy 44
RM SL54B05

NACA

RESEARCH MEMORANDUM

for the

Bureau of Aeronautics, Department of the Navy

RESULTS OF FREE-FLIGHT TEST OF 1/10-SCALE MODEL OF THE
CONVAIR XF2Y-1 AIRPLANE BETWEEN MACH NUMBERS OF 0.7
AND 1.45, INCLUDING POWER-ON FLIGHT AT
MACH NUMBER 1.2

REPORT NO. NACA DE 365

UNCLASSIFIED

By William M. Bland, Jr.

Langley Aeronautical Laboratory
Langley Field, Va.

*NASA TPA 7 Effective 5-29-59
NB 7-7-59*

CLASSIFIED DOCUMENT

This material contains information affecting the National Defense of the United States within the meaning of the espionage laws, Title 18, U.S.C., Secs. 793 and 794, the transmission or revelation of which in any manner to an unauthorized person is prohibited by law.

NATIONAL ADVISORY COMMITTEE FOR AERONAUTICS WASHINGTON

~~CONFIDENTIAL~~



NATIONAL ADVISORY COMMITTEE FOR AERONAUTICS

RESEARCH MEMORANDUM

for the

Bureau of Aeronautics, Department of the Navy

RESULTS OF FREE-FLIGHT TEST OF 1/10-SCALE MODEL OF THE

CONVAIR XF2Y-1 AIRPLANE BETWEEN MACH NUMBERS OF 0.7

AND 1.45, INCLUDING POWER-ON FLIGHT AT

MACH NUMBER 1.2

TED NO. NACA DE 365

By William M. Bland, Jr.

SUMMARY

A 1/10-scale model of the Convair XF2Y-1 airplane containing a solid-fuel rocket motor designed to simulate full-scale turbojet engine characteristics with full afterburning at a Mach number of 1.2 and an altitude of 35,000 feet has been tested in free flight to a maximum Mach number of 1.45. The engine inlets were closed with approximately spherical fairings.

Results of the flight indicate that, in general, the lift-curve slope, the static-longitudinal-stability derivative, the aerodynamic-center location, and the combined damping-in-pitch derivatives agreed with the results obtained from the flight of a model with open inlets. At the higher Mach numbers the model appeared to have slight dynamic lateral instability, but improvement was noted with decreasing Mach number and increasing trim angle of attack. Also, values of the total drag coefficient of this model were higher at subsonic and supersonic speeds than those obtained for a model with open inlets.

The jet exhaust from the rocket motor, which operated for a short time near a Mach number of 1.2, increased the suction forces at the base and on the rear portion of the fuselage aft of the exits and increased the nose-down pitching-moment coefficient contributed by the portion of the fuselage aft of the exits from approximately -0.0034 to approximately -0.0048.

INTRODUCTION

Flight tests of rocket-propelled models of the Convair XF2Y-1 airplane at high subsonic, transonic, and supersonic speeds, as requested by the Bureau of Aeronautics, Department of the Navy, have been continued by the Langley Pilotless Aircraft Research Division with the flight of a model with closed inlets. Results of the power-on flight at $M = 1.53$ of another model with closed inlets are presented in reference 1. Presented in reference 2 are the results of the flight of a model with open inlets.

The Convair XF2Y-1 airplane, which is a tailless configuration with thin modified-delta wing and vertical surfaces designed to be a water-based supersonic fighter airplane, has twin-turbojet engines which exhaust over a portion of the fuselage aft of the exits (hereinafter referred to as beach areas, or beaches). During a portion of the present flight a solid-fuel rocket motor contained within the fuselage of the model was used to simulate the characteristics of the turbojet engines of the full-scale airplane at $M = 1.2$ at an altitude of 35,000 feet to determine the effect of exhaust flow on the beach areas. Drag and stability results were also obtained during the flight.

The flight was made at the Pilotless Aircraft Research Station, Wallops Island, Va.

SYMBOLS

S	area, sq ft
b	wing span, ft
\bar{c}	wing mean aerodynamic chord, ft
A	cross-sectional area of equivalent body, sq ft
r_{equi}	radius of equivalent body of revolution, ft
D_{max}	maximum diameter of equivalent body, ft
l	body length, ft
X	distance from nose, ft
X_{cg}	nondimensional center-of-gravity location, percent \bar{c}

CONFIDENTIAL

M	Mach number
V	velocity, ft/sec
R	Reynolds number, based on \bar{c}
m	mass flow
q_0	free-stream dynamic pressure, lb/sq ft
α	angle of attack, deg
t	time, sec
$\dot{\alpha}$	rate of change of angle of attack with time, $\frac{d\alpha}{dt} \frac{1}{57.3}$
β	angle of sideslip, deg
θ	angle of pitch, deg
$\dot{\theta}$	rate of change of angle of pitch with time, $\frac{d\theta}{dt} \frac{1}{57.3}$
p	static pressure, lb/sq in
P	pressure coefficient, $144 \frac{p - p_a}{q_0}$
H	total pressure, lb/sq in
C_N	normal-force coefficient, $\frac{\text{Normal force}}{q_0 S_w}$
C_C	chord-force coefficient, $\frac{\text{Chord force}}{q_0 S_w}$
C_Y	side-force coefficient, $\frac{\text{Side force}}{q_0 S_w}$
C_T	thrust coefficient, $\frac{\text{Thrust}}{q_0 S_w}$

C_n	yawing-moment coefficient, $\frac{\text{Yawing moment}}{q_0 S_w b}$
C_m	pitching-moment coefficient, $\frac{\text{Pitching moment}}{q_0 S_w \bar{c}}$
C_D	drag coefficient, $\frac{\text{Drag}}{q_0 S_w}$
C_L	lift coefficient, $\frac{\text{Lift}}{q_0 S_w}$
$C_{L\alpha}$	lift-curve slope, $\frac{dC_L}{d\alpha}$
$C_{m\alpha}$	static-longitudinal-stability derivative, $\frac{dC_m}{d\alpha}$
X_{ac}	aerodynamic-center location, $X_{cg} - 100 \frac{C_{m\alpha}}{C_{L\alpha}}$, percent \bar{c}
$C_{n\beta}$	static-directional-stability derivative, per deg
$C_{mq} + C_{m\dot{\alpha}}$	combined damping-in-pitch derivatives, per radian
$C_{mq} = \frac{dC_m}{d\left(\frac{q\bar{c}}{2V}\right)}$	
$C_{m\dot{\alpha}} = \frac{dC_m}{d\left(\frac{\dot{\alpha}\bar{c}}{2V}\right)}$	

Subscripts:

w	wing
e	exit
a	atmospheric
t	trim

MODEL DESCRIPTION

The general characteristics of the model are shown in the drawing in figure 1, in the photographs in figure 2, and in table I. The area distribution of the model and the profile of a body of revolution with an equivalent area distribution are shown in figure 3.

The wings were constructed of laminated wood with aluminum-alloy chord-plane stiffeners and inlays under the wing surface. The construction of the vertical tail was similar except that 0.032-inch Inconel plates were inlaid, in both sides, over a large portion of the tail as shown in figure 2. The elevons, which were full-span, were deflected 4.2° , trailing edge up, so the model would trim at a positive angle of attack. The rudder was not deflected.

The duct inlets on this model were closed with approximately spherical covers (fig. 2(a)) and the space allotted for turbojet engines and ducting in the full-scale airplane was used to house a solid-fuel rocket motor as described in reference 1. This rocket motor was designed to simulate the scale mass flow, exit pressure ratio, and thrust of the full-scale turbojet engines at $M = 1.2$ at an altitude of 35,000 feet with full afterburning.

Instruments were installed in the nose, above the wing ahead of the rocket motor, and below the wing in the same manner as the instrument installation described in reference 1. The instruments, which were 14 in number, were used to measure angle of attack, accelerations along each of the body axes, total and static pressures, rocket-chamber pressure, base pressure, and some pressures over the port beach. The locations of the orifices for measuring base and beach pressures are shown in figure 4.

TEST PROCEDURES

The model and booster assembly were launched from a mobile-type launcher inclined at an angle of approximately 60° above the horizontal, as shown in figure 5. After being accelerated to a Mach number slightly less than 1.5 by the booster rocket motor, the model separated from the booster assembly and coasted in free flight, being decelerated by drag and its weight component along the flight path. After an interval of coasting flight calculated to be long enough for the model to decelerate to $M \approx 1.2$, the rocket motor contained within the model, was ignited. After completion of rocket-motor burning, the model resumed coasting flight and decelerated through the speed range.

During the intervals of coasting flight the model was disturbed in pitch by pulse rockets which were located in the rear of the model in the lower part of the fuselage.

During the flight of the model, information from each instrument contained within the model was transmitted from the model to the ground receiving station where it was recorded. At the ground station a radar tracking unit was used to determine the position of the model in space. A radiosonde was used to measure atmospheric conditions at the time of the flight.

The variation of Reynolds number, which was based on \bar{c} , with Mach number is shown in figure 6.

ACCURACY

Systematic errors in the various measured quantities due to inherent limitations in the measuring, recording, and data-reduction systems are estimated to be within ± 1 percent of full-scale instrument calibration which results in the following limits:

M	ΔC_N	ΔC_C	ΔC_Y	ΔP	$\Delta \alpha$
1.4	± 0.002	± 0.001	± 0.002	± 0.005	± 0.09
1.1	$\pm .004$	$\pm .001$	$\pm .003$	$\pm .010$	$\pm .09$
.8	$\pm .008$	$\pm .002$	$\pm .005$	$\pm .020$	$\pm .09$

However, the accuracy of other quantities, such as slopes, which were obtained by fairing through data points, is believed to be better than that implied by the accuracy of the individual quantities.

Systematic errors in Mach number, which was calculated from p_a and H , are estimated to be within ± 0.005 at the highest Mach number of the test and ± 0.020 at the lowest Mach number.

RESULTS AND DISCUSSION

Time histories of some of the basic quantities resulting from measurements made during the flight of the model in a time interval that included rocket-motor operation are presented in figure 7. Oscillations of the quantities α and C_N indicate the behavior of the model as it recovered from changes in longitudinal trim that were caused by rocket-motor operation and by the cessation of rocket-motor operation. Additional short-period oscillations of greater amplitude than those shown

in figure 7 were obtained when the model recovered from an abrupt change in trim at the time it separated from the booster assembly and when the model recovered from disturbances due to pulse rockets at approximately 3.8 seconds and 7.5 seconds after model take-off.

Stability Characteristics

Longitudinal.— The model was equipped with two instruments for measuring normal acceleration, one in the nose and one aft of the center of gravity; therefore, it was possible to determine pitching acceleration and the total instantaneous pitching-moment coefficient. Typical variations of C_L and C_m with α are shown in figures 8 and 9, respectively. Values of $C_{L\alpha}$ and $C_{m\alpha}$, as obtained by applying the least-squares method to the complete range of data obtained during the first three or four oscillations following a disturbance, are shown in figures 10(a) and 10(b), respectively. It can be seen that the $C_{L\alpha}$ values obtained during power-on flight are apparently higher than those obtained at about the same Mach number in coasting flight; however, the scatter in the data makes this observation uncertain. Also included in figure 10(b) are values of $C_{m\alpha}$ calculated by applying the average period obtained for each set of angle-of-attack oscillations to the method used in reference 3.

By using values of $C_{L\alpha}$ and $C_{m\alpha}$, figures 10(a) and 10(b), it was possible to compute the aerodynamic-center locations shown in figure 10(c), which show that the aerodynamic-center location remained about constant in the Mach number range for which data were obtained.

Further analysis of the angle-of-attack oscillations by a method included in reference 3 resulted in the combined damping-in-pitch derivatives presented in figure 10(d). The value for the power-on condition, which appeared low, was calculated using an average power-on value of $C_{L\alpha}$; however, using a $C_{L\alpha}$ value from the faired curve (fig. 10(a)) at $M = 1.186$ only increased $C_{m\dot{q}} + C_{m\dot{\alpha}}$ to -0.348 .

Compared with the results presented in reference 2, as obtained for the model with open inlets, the longitudinal-stability parameters $C_{L\alpha}$, $C_{m\alpha}$, X_{ac} , and $C_{m\dot{q}} + C_{m\dot{\alpha}}$ obtained during the present test are about the same except for $C_{L\alpha}$, which appears about 10 percent lower near $M \approx 1.2$, and X_{ac} which is larger, that is, the aerodynamic center is slightly farther back along the mean aerodynamic chord in the supersonic region investigated.

Lateral.- The time history of the side-force coefficient, a portion of which is included in figure 7, contained oscillations apparently resulting from a component of the disturbances in pitch. These oscillations, which were somewhat irregular and of much lower amplitude than those of the normal-force coefficient, increased slightly in amplitude between $M \approx 1.45$ and $M \approx 1.18$ (first coasting period) with the center of gravity at 20.65 percent \bar{x} , indicating that the model had dynamic lateral instability. During and after rocket-motor operation, the oscillations of the side-force coefficient, which were convergent, indicated dynamic lateral stability. The dynamic lateral stability, as indicated by the damping of the side-force-coefficient oscillations, was increased as the Mach number decreased. Coincident with the decrease in Mach number there was an increase in the trim angle of attack (fig. 11) which, as was shown in reference 1, increases the dynamic lateral stability.

Values of the directional-stability parameter as calculated by applying the average period of each set of oscillations to the single-degree-of-freedom method, which has been applied to another tailless configuration in reference 4, are as follows:

Mach number	$C_{n\beta}$ /degree
1.22	0.0011
1.18	.0017 (rocket-motor operation)
1.06	.0019
.93	.0021

Trim Characteristics

The variations with Mach number of the trim angle of attack and the trim lift coefficient obtained during the periods of coasting flight are shown in figure 11. The effect of rocket-motor operation on these trim conditions is also noted in figure 11.

Presented in figure 12 is the variation of the total drag coefficient with Mach number for the trim conditions of the test. While the transonic drag rise in the region $0.8 \leq M \leq 1.1$ is approximately the same as that obtained for the model with open inlets, reference 2, the total drag coefficients at subsonic and supersonic speeds are about 10 percent higher. The minimum drag coefficient obtained for another model with the same inlet fairings (ref. 1) at $M = 1.53$, as shown in figure 12, compares with the results of the present test.

Effect of Rocket Exhaust Over the Beaches

The solid-fuel rocket motor contained within the model, which was designed to simulate the thrust and exit flow conditions of the turbojet engines of the full-scale airplane with full afterburning at a Mach number of 1.2 at an altitude of 35,000 feet, supplied about constant thrust between $t \approx 5.3$ seconds and $t \approx 6.35$ seconds after take-off. During this time interval the model was accelerated from $M \approx 1.17$ to $M \approx 1.22$ (fig. 7). A comparison of model rocket motor and airplane engine characteristics is given in the following table (characteristics of the rocket motor were obtained from static ground test):

	S_e	M_e	C_T	$\frac{H_e}{Pa}$	$\frac{m_e}{m_a}$
1/10-scale rocket model	0.01979	1.0	0.051	6.4	0.97
Airplane at $M = 1.2$; altitude, 35,000 ft; full afterburning	1.979	1.0	.038	5.8	.77

Throughout the flight of the model, pressure measurements were made on the port exit annulus and on the port beach at the stations indicated in figure 4. The measured pressures transformed into pressure-coefficient form are presented in figure 13 as functions of Mach number. The effect of rocket-motor exhaust on the values of the pressure coefficients is shown at $M = 1.2$. Also included in figure 13 are the pressure coefficients for the power-on condition at $M = 1.53$ as obtained from reference 1.

The base-drag coefficient, which was calculated by assuming that the pressure measured on the port exit annulus was representative of the pressure on the starboard annulus and across the exit areas when the rocket motor was not operating, is presented in figure 14. Also included in figure 14 are the lift and drag coefficients contributed by the beaches (port and starboard). It is shown that the effect of rocket-motor exhaust at $M = 1.2$ was to increase $C_{D(\text{beach})}$ by approximately 35 percent and $C_{L(\text{beach})}$ by approximately 40 percent. A similar increase in $C_{D(\text{base})}$ could be noted if the base forces for power-on and power-off conditions were computed for the same areas; however, the power-on base-drag coefficients were computed for only the annular areas around the exits. In figure 15 it is shown that the pitching-moment coefficient contributed by the beaches was increased (negatively) by about 40 percent by rocket-motor exhaust at $M = 1.2$. Also included in figures 14 and 15 are the values $C_{D(\text{base})}$, $C_{D(\text{beach})}$, $C_{L(\text{beach})}$, and $C_{m(\text{beach})}$ obtained for power-on flight at $M = 1.53$ (ref. 1) which are

generally of the same magnitude as the corresponding coefficients obtained for the power-on condition of the present test.

The coefficients pertaining to the beaches were determined by the method presented in reference 1. The assumption in reference 1 that treated the variation of the pressure aft of the rear orifice on the beach has been assayed. It was determined that the values of the coefficients pertaining to the beaches remained essentially unchanged if the pressure was assumed to remain constant or if the pressure was assumed to return linearly to atmospheric pressure at the rearmost boundaries of the beaches.

Some idea of the general effect of the ratio of the jet total pressure to atmospheric static pressure on the magnitude of the base-pressure coefficient can be obtained from reference 5 which includes information on incomplete boattail configurations with exit diameter equal to 0.71 times the base diameter (approximately 0.69 for the present test). The results in reference 5, which are presented only for $M = 1.91$, show that changing the ratio H_e/p_a from 6.4 (the value obtained in the present test) to 5.8 (the value desired for turbojet simulation) would make the base-pressure coefficient approximately 15 percent more negative. Although other unknown factors such as Mach number effects, lack of symmetry at the exits, and boundary-layer effects make any quantitative adjustment of the pressure coefficient to correspond to the desired value of H_e/p_a impossible, it is believed that the results of the present test, while possibly not giving the true magnitude of the pressure coefficients, are at least indicative of the jet effects.

Also, as discussed in reference 5, small amounts of air flow out of the base annulus, which is probably the case for full-scale airplanes, can change the base-pressure coefficient considerably.

CONCLUDING REMARKS

A 1/10-scale model of the Convair XF2Y-1 airplane with closed inlets has been flown to a maximum Mach number of 1.45. In general, the lift-curve slope, the static-longitudinal-stability derivative, the aerodynamic-center location, and the combined damping-in-pitch derivatives agreed with the results obtained from the flight of a similar model with open inlets. Between $M \approx 1.45$ and $M \approx 1.18$ the model appeared to have slight lateral dynamic instability, but improvement was noted as the Mach number decreased and the trim angle of attack increased. The values of the total drag coefficient obtained for this model, which had spherical covers closing the inlets, were higher at both subsonic and supersonic speeds than those obtained for the model with open inlets.

A rocket motor contained in the model designed to simulate the thrust and exit flow conditions of the turbojet engines of the full-scale airplane was operated for a short time near $M = 1.2$. It was determined that the jet exhaust from the rocket motor increased the suction forces at the base and on the rear portion of the fuselage aft of the exits and increased the nose-down pitching-moment coefficient contributed by the rear portion of the fuselage aft of the exits from approximately -0.0034 to approximately -0.0048 .

Langley Aeronautical Laboratory,
National Advisory Committee for Aeronautics,
Langley Field, Va., January 20, 1954.


William M. Bland, Jr.
Aeronautical Research Scientist

Approved:


Joseph A. Shortal
Chief of Pilotless Aircraft Research Division

DY

REFERENCES

1. Bland, William M., Jr., and Nelson, Robert L.: Results of a Power-On Flight of a 1/10-Scale Rocket-Propelled Model of the Convair XF2Y-1 Airplane at a Mach Number of 1.53 - TED No. NACA DE 365. NACA RM SL53I30A, Bur. Aero., 1953.
2. Welsh, Clement J., Bland, William M., Jr., and Walters, Richard E.: Rocket-Model Investigation of the Longitudinal Stability and Drag Characteristics of a 1/10-Scale Model of the Convair XF2Y-1 Airplane Having Open Ducts and the Elevons Deflected Upward 3.5° - TED No. NACA DE 365. NACA RM SL54A05, Bur. Aero., 1954.
3. Gillis, Clarence L., Peck, Robert F., and Vitale, A. James: Preliminary Results From a Free-Flight Investigation at Transonic and Supersonic Speeds of the Longitudinal Stability and Control Characteristics of an Airplane Configuration With a Thin Straight Wing of Aspect Ratio 3. NACA RM L9K25a, 1950.
4. Purser, Paul E., and Mitchell, Jesse L.: Miscellaneous Directional-Stability Data for Several Airplane-Like Configurations From Rocket-Model Tests at Transonic Speeds. NACA RM L52E06b, 1952.
5. Cortright, Edgar M., Jr., and Schroeder, Albert H.: Investigation at Mach Number 1.91 of Side and Base Pressure Distributions Over Conical Boattails Without and With Jet Flow Issuing From Base. NACA RM E51F26, 1951.

TABLE I

GENERAL CHARACTERISTICS OF THE THIRD 1/10-SCALE ROCKET-PROPELLED

MODEL OF THE CONVAIR XF2Y-1

Wing:

Total included area, sq ft	5.63
Span, ft	3.37
Mean aerodynamic chord, ft	2.14
Aspect ratio	2.03
Airfoil section:	
At center line	NACA 0002.89-65 (modified)
From 86 percent of half-span to tip	NACA 0004-65 (modified)

Tail:

Exposed area, sq ft	0.80
Airfoil section:	
At root	NACA 0003-65 (modified)
At tip	NACA 0004-65 (modified)

Elevon deflections, trailing edge up, deg 4.2

Weight:

With rocket propellant, lb	115
Without rocket propellant, lb	110

Moment of inertia about body axis, slug-ft²:

With rocket propellant:	
Roll	0.46
Yaw	6.61
Pitch	6.05
Without rocket propellant:	
Roll	0.44
Yaw	6.49
Pitch	6.01

Center-of-gravity positions:

With rocket propellant:	
Longitudinal, percent M.A.C.	20.65
Vertical, in. above reference line	0.94
Without rocket propellant:	
Longitudinal, percent M.A.C.	19.45
Vertical, in. above reference line	0.84

Rocket-thrust-line position, in. above reference line 2.6

TABLE I. - Concluded

GENERAL CHARACTERISTICS OF THE THIRD 1/10-SCALE ROCKET-PROPELLED

MODEL OF THE CONVAIR XF2Y-1

Angle principal axis rotated below body axis at nose, deg	
With rocket propellant	$1\frac{1}{2}$
Without rocket propellant	$1\frac{1}{4}$
Annular area about both exits, sq in	5.88



(a) Three-quarter front view. L-80934.1

Figure 2.- External views of the model.

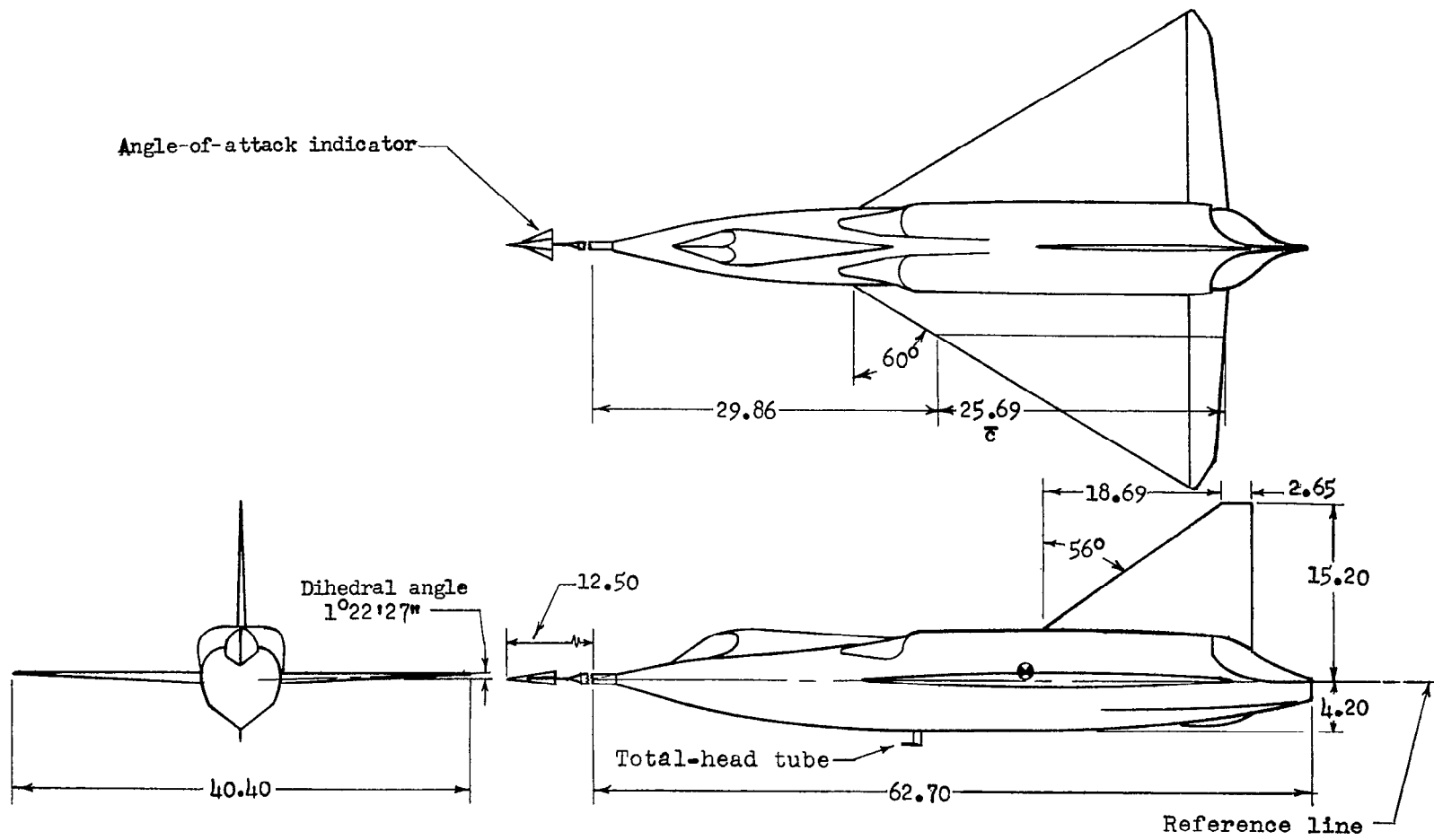
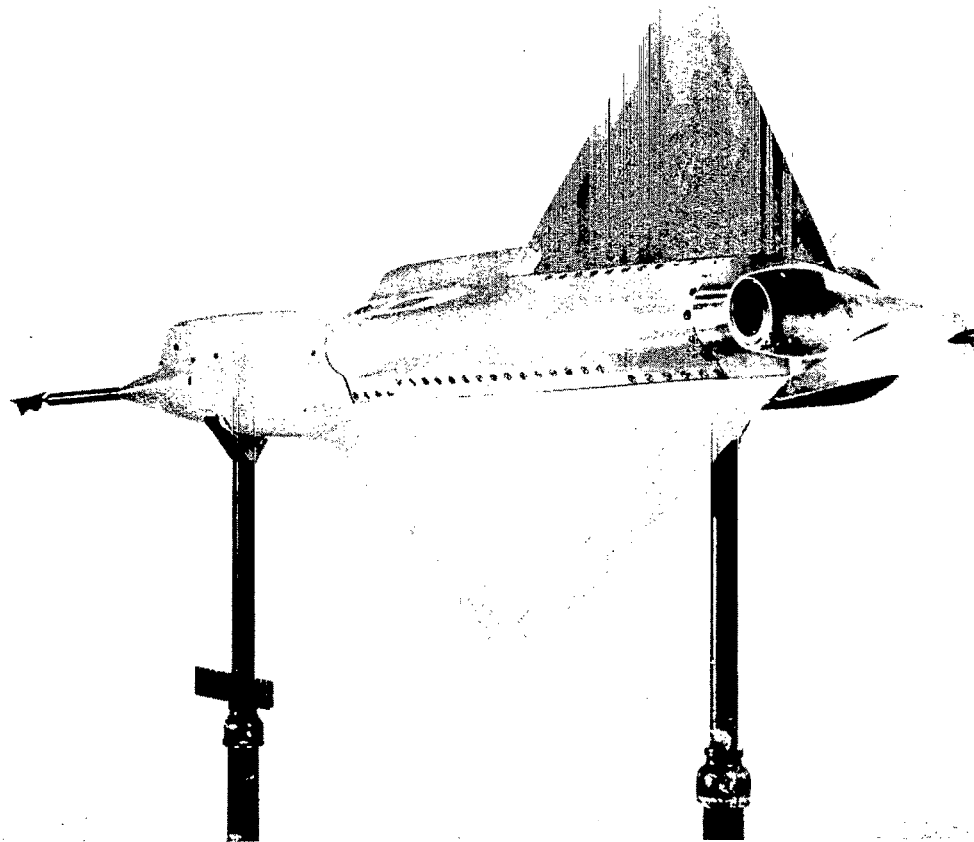


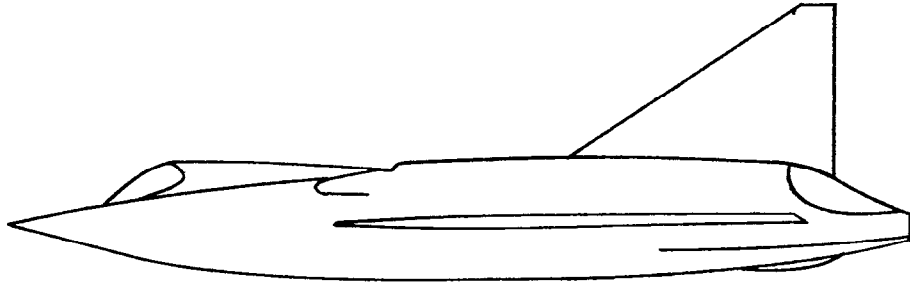
Figure 1.- General arrangement of model. All linear dimensions in inches.



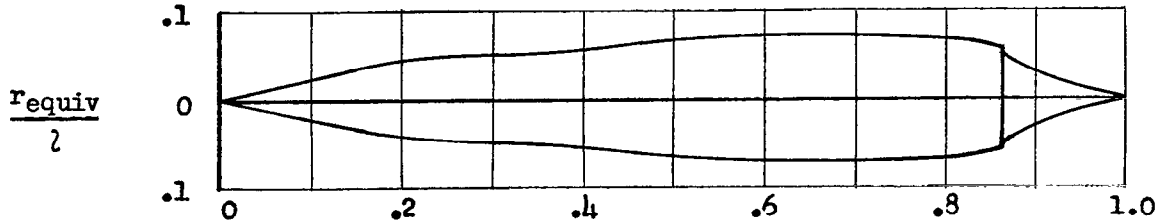
(b) Three-quarter rear view. L-77631.2

Figure 2.- Concluded.

~~CONFIDENTIAL~~



Model



$\frac{x}{\lambda}$

Equivalent body, $\frac{\lambda}{D_{max}} = 6.98$
 $\lambda = 62.7$ inches for 1/10-scale model

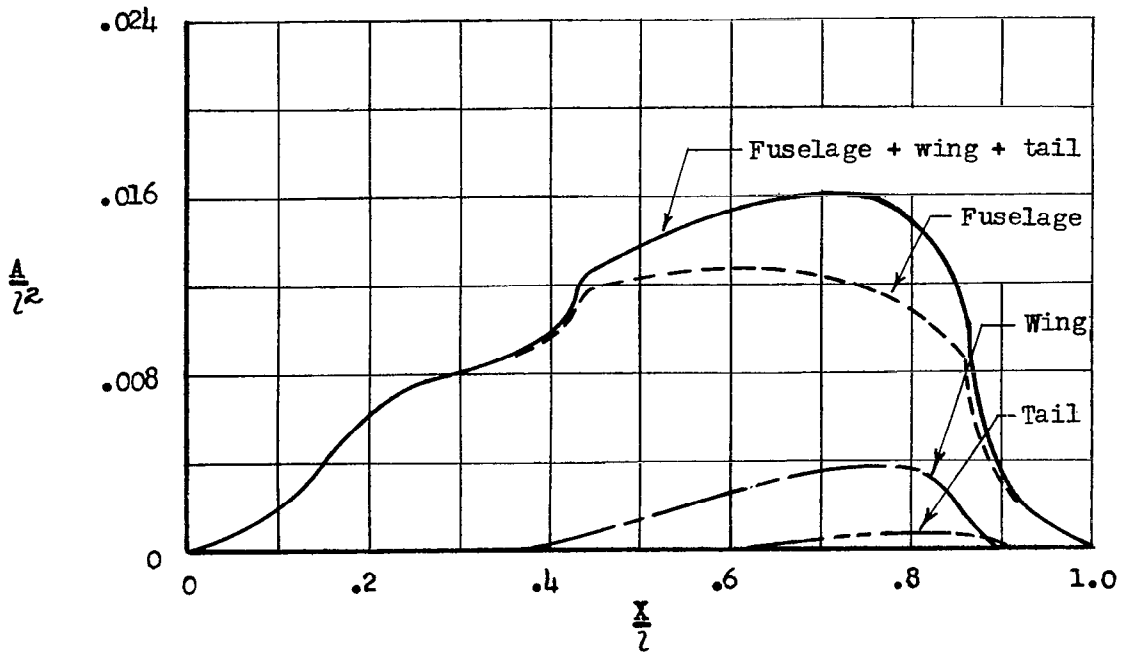
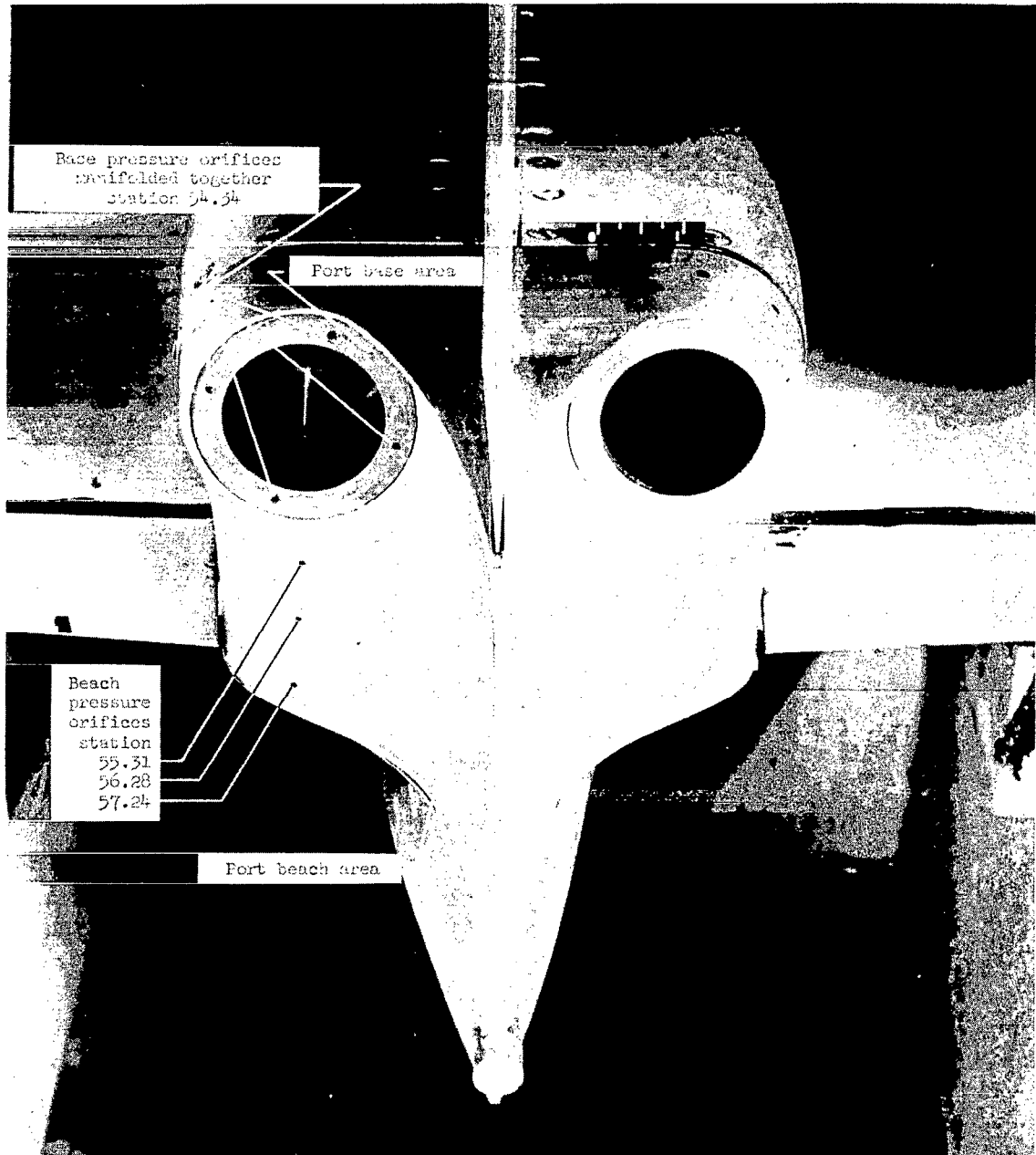


Figure 3.- Area distribution of model including area of closed ducts and profile of body of revolution with equivalent area distribution.

~~CONFIDENTIAL~~



L-78839.2

Figure 4.- Aft end of the model showing the base and beach pressure orifices.

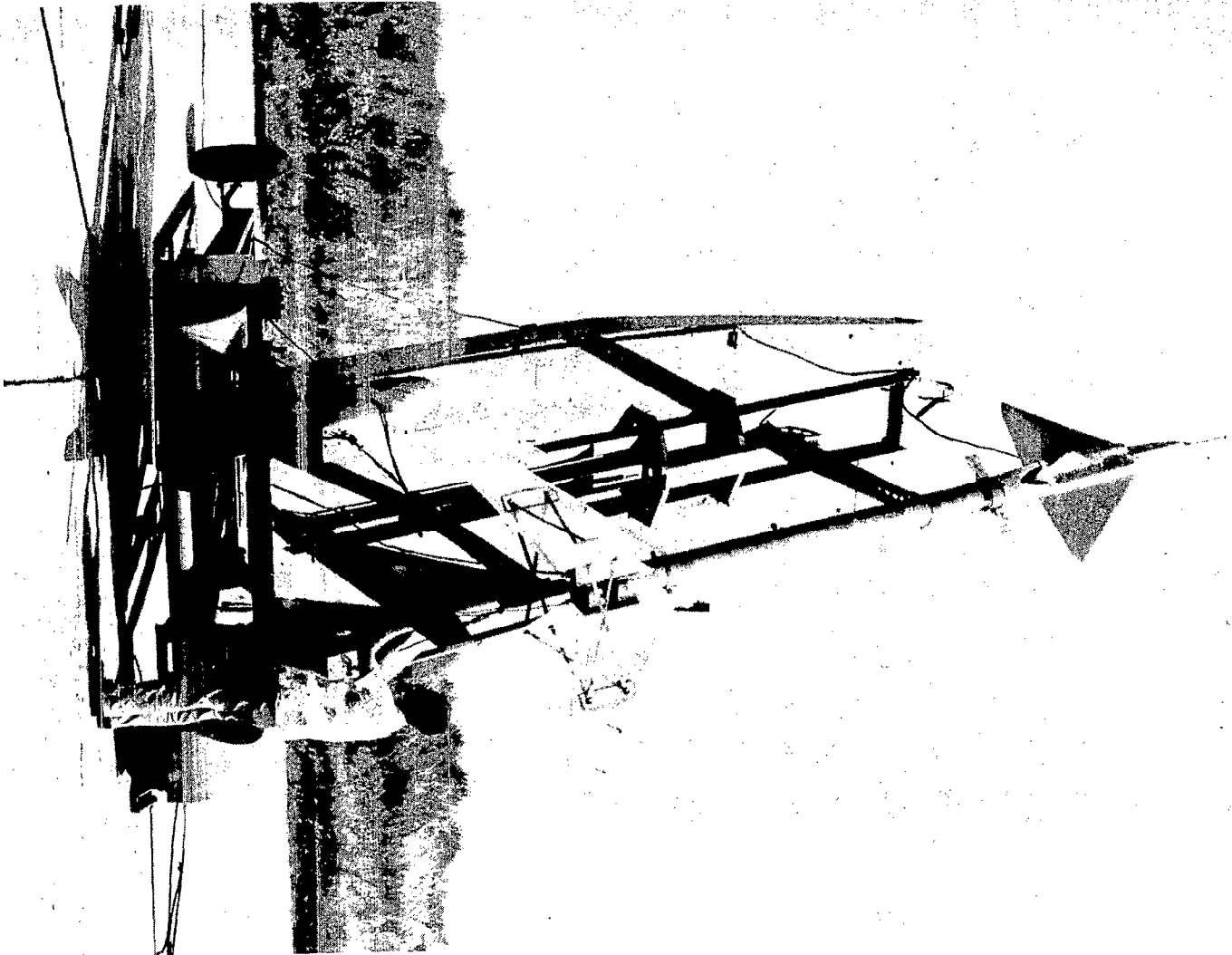


Figure 5.- Model and booster assembly on mobile launcher. L-81321.1

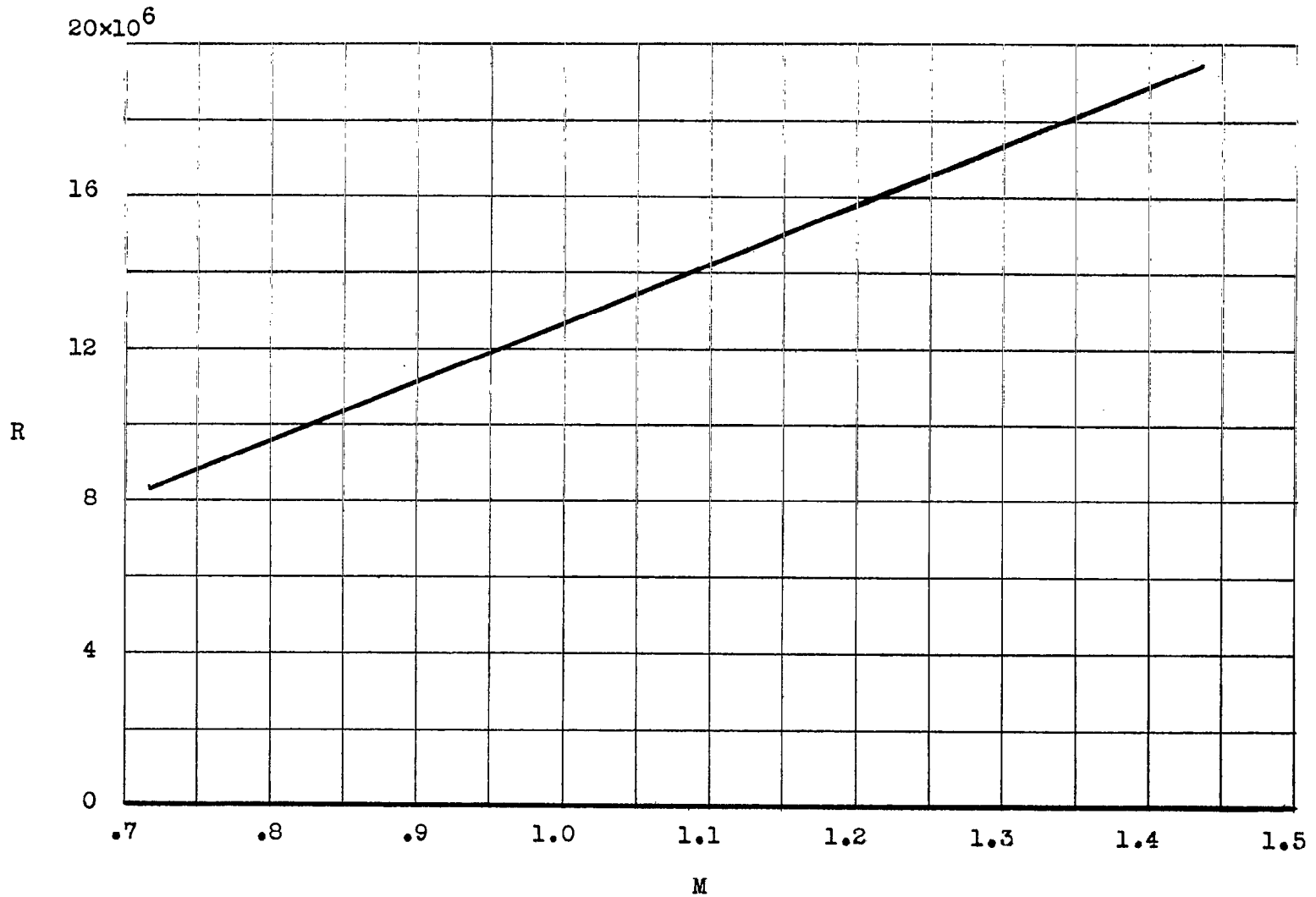


Figure 6.- Variation of the Reynolds number, based on the mean aerodynamic chord, with Mach number.

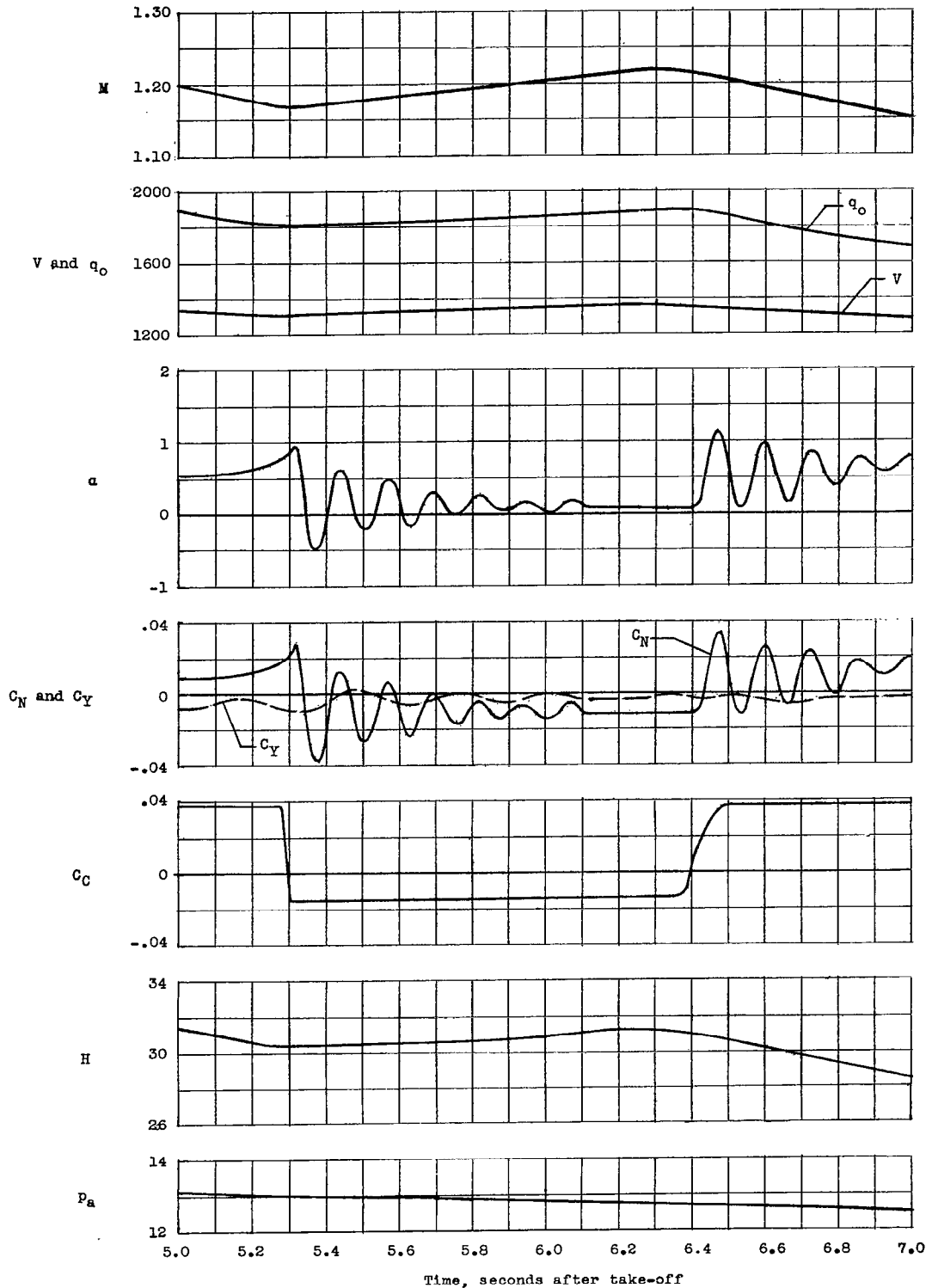


Figure 7.- Time histories of some of the quantities measured in time interval that included rocket-motor operation.

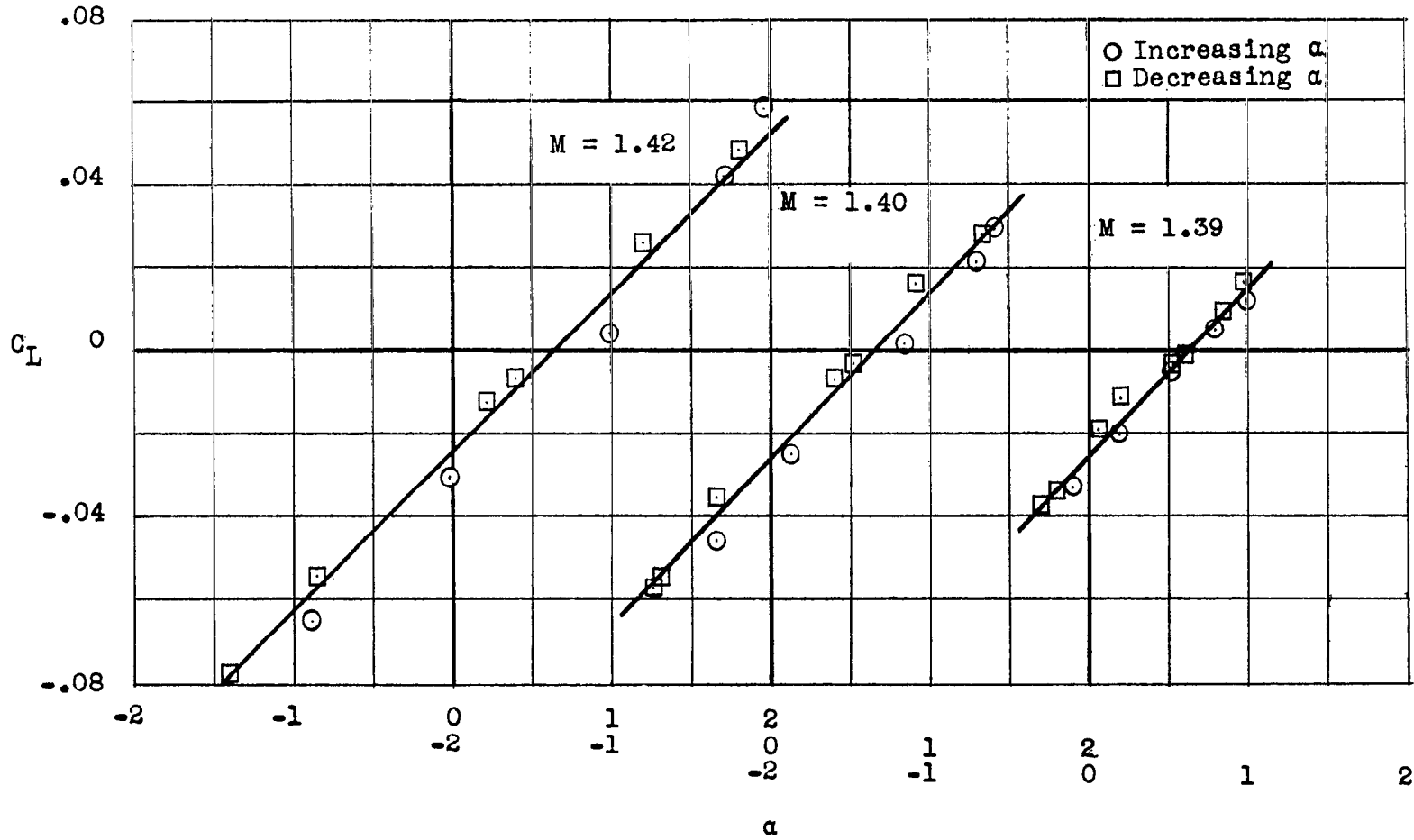


Figure 8.- Typical variation of lift coefficient with angle of attack.

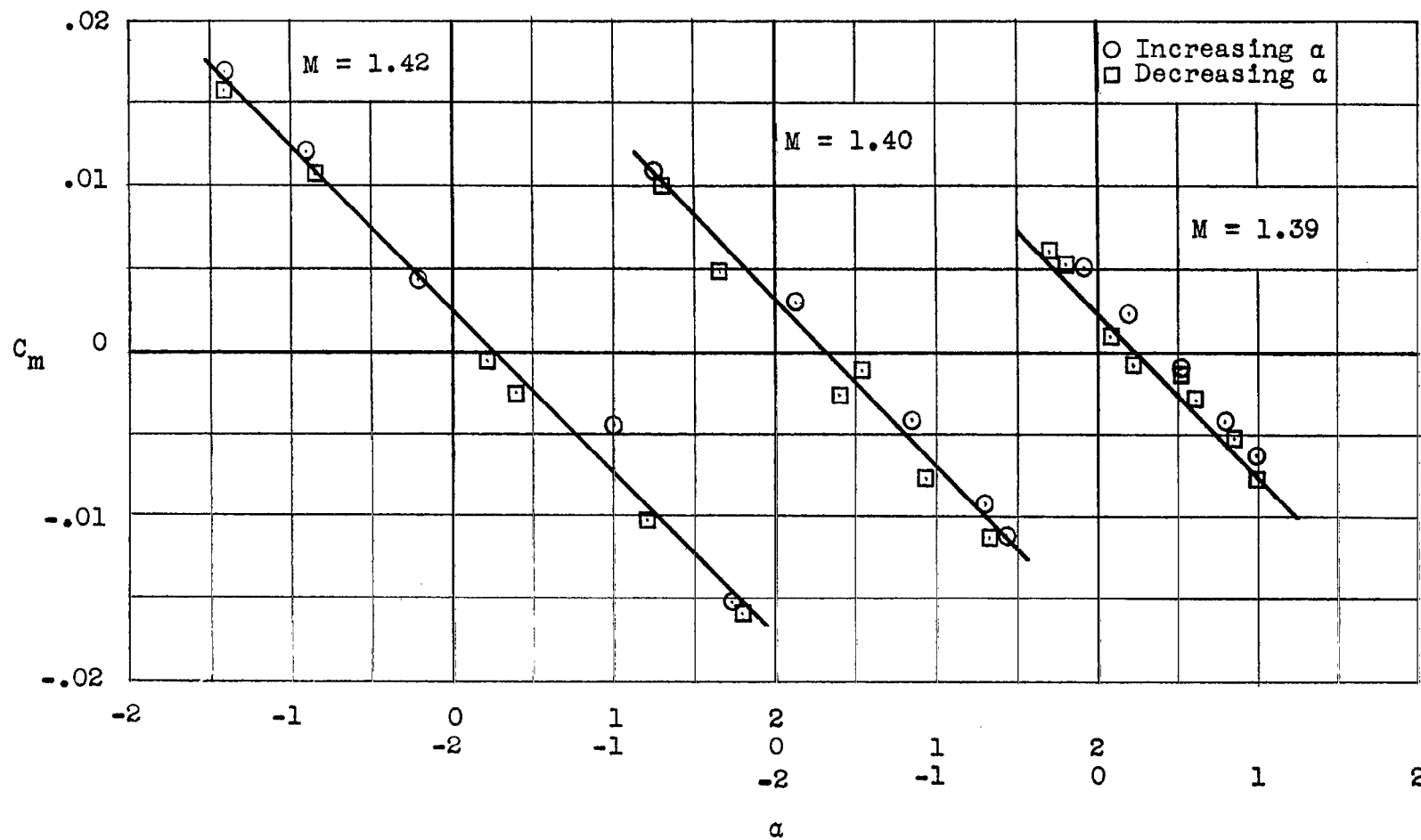
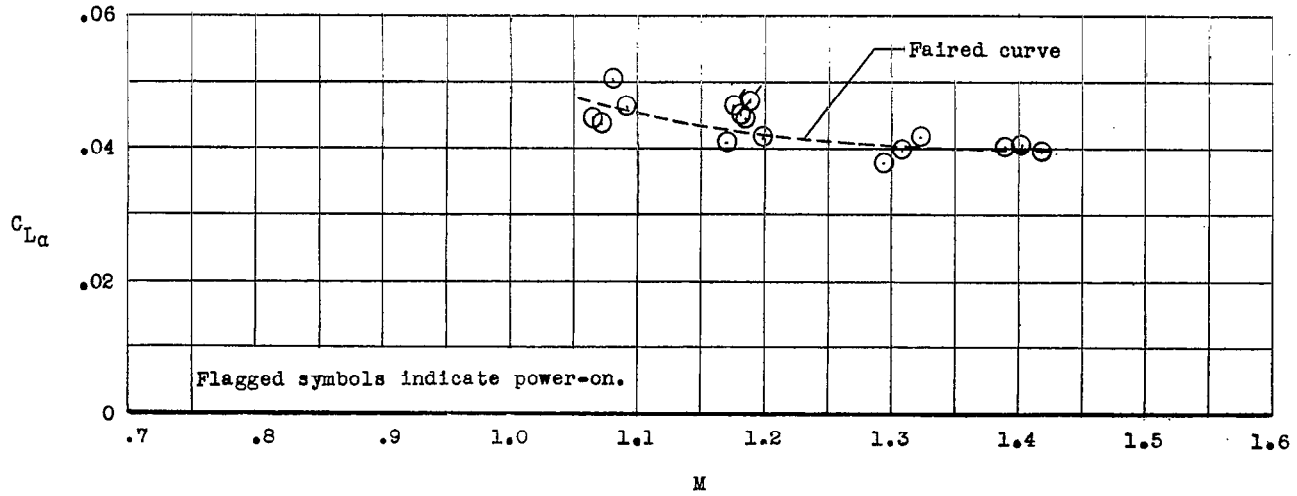
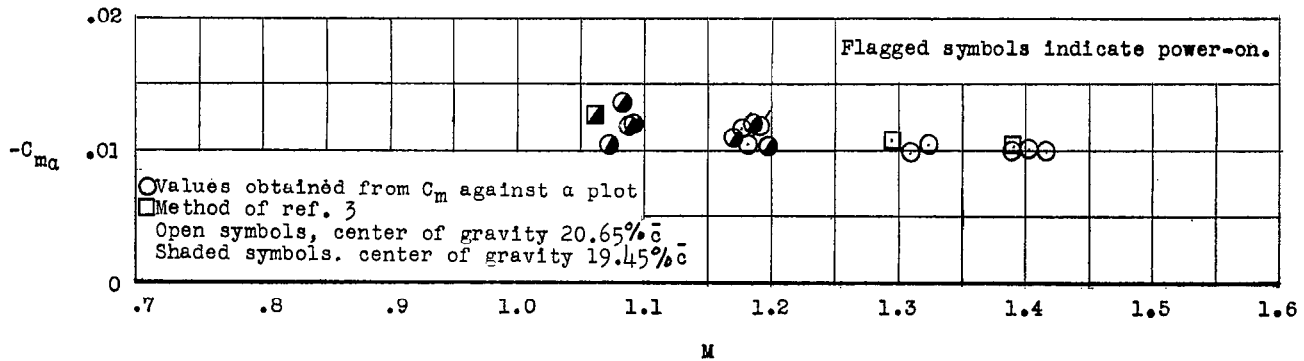


Figure 9.- Typical variation of total pitching-moment coefficient with angle of attack. Center of gravity at 20.65 percent mean aerodynamic chord.

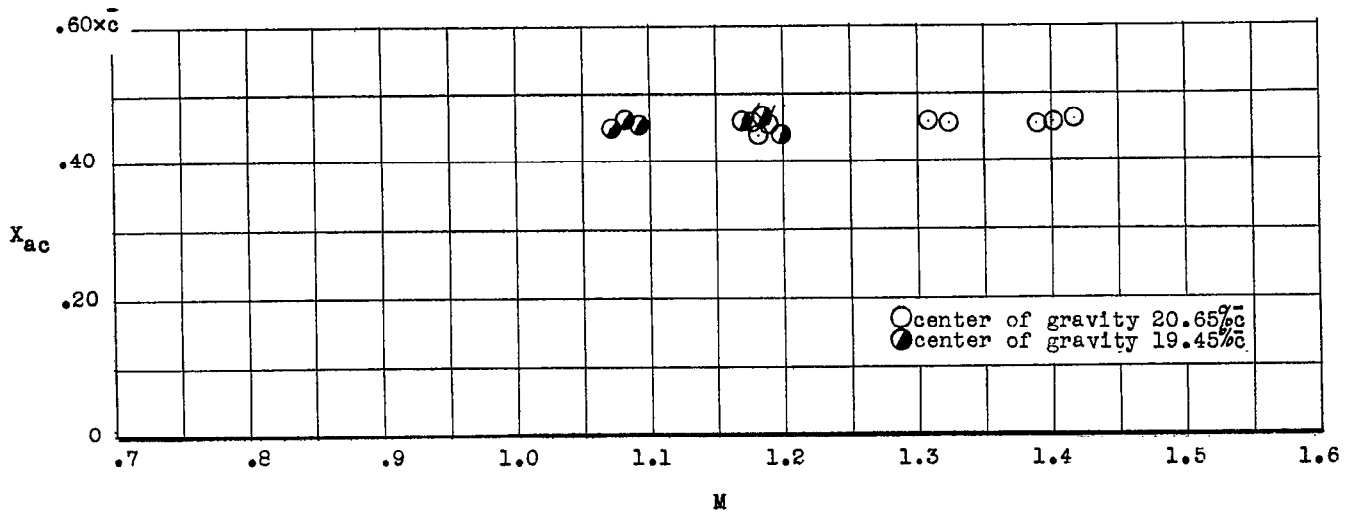


(a) Slope of the lift curve.

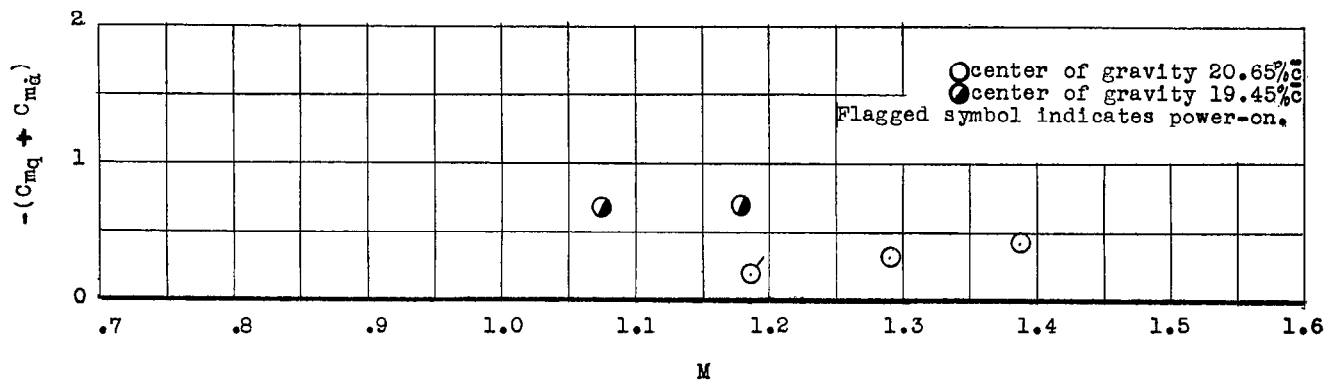


(b) Static-longitudinal-stability derivative.

Figure 10.- The variation with Mach number of the longitudinal-stability parameters.



(c) Aerodynamic-center location.



(d) Damping-in-pitch derivatives.

Figure 10.- Concluded.

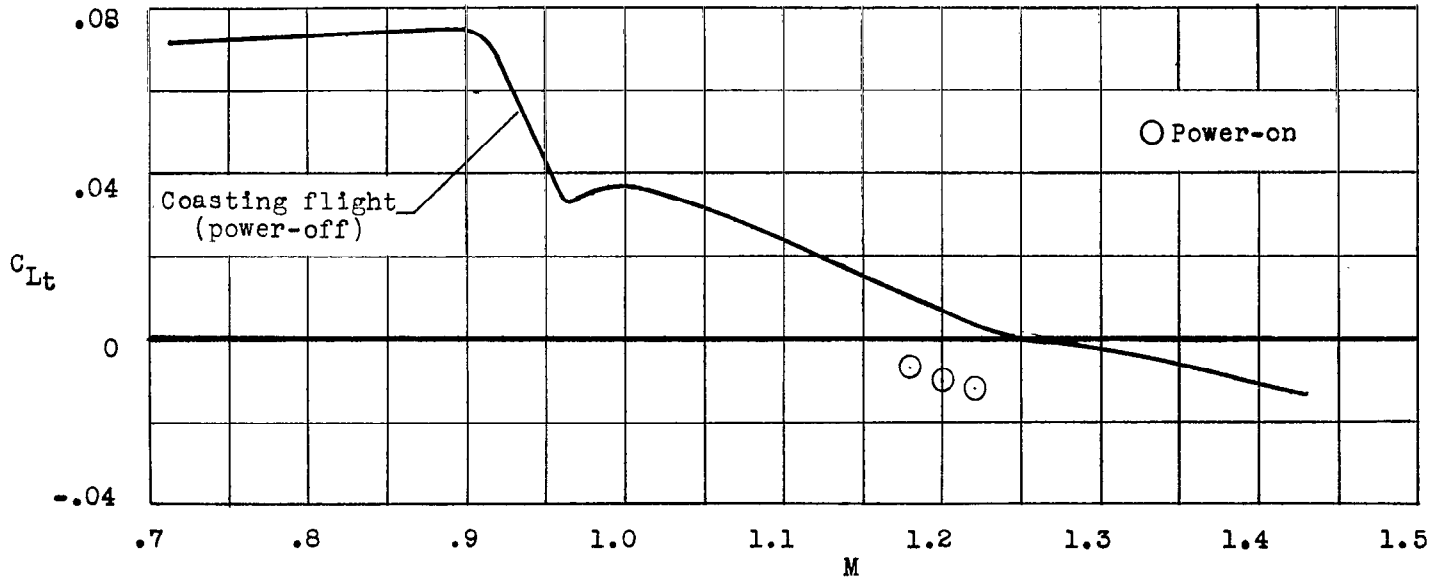
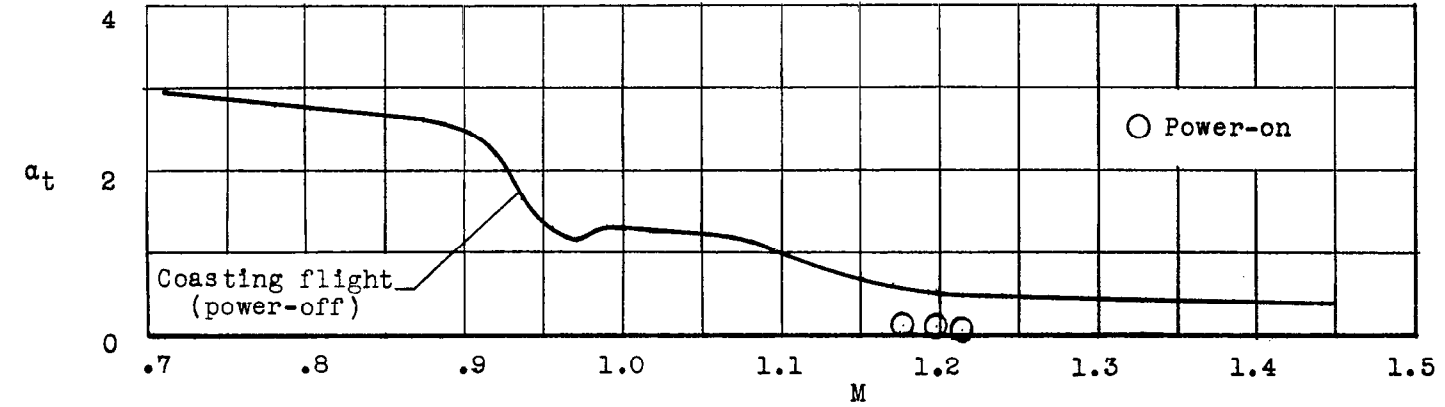


Figure 11.- The variation with Mach number of the trim angle of attack and the trim lift coefficient.

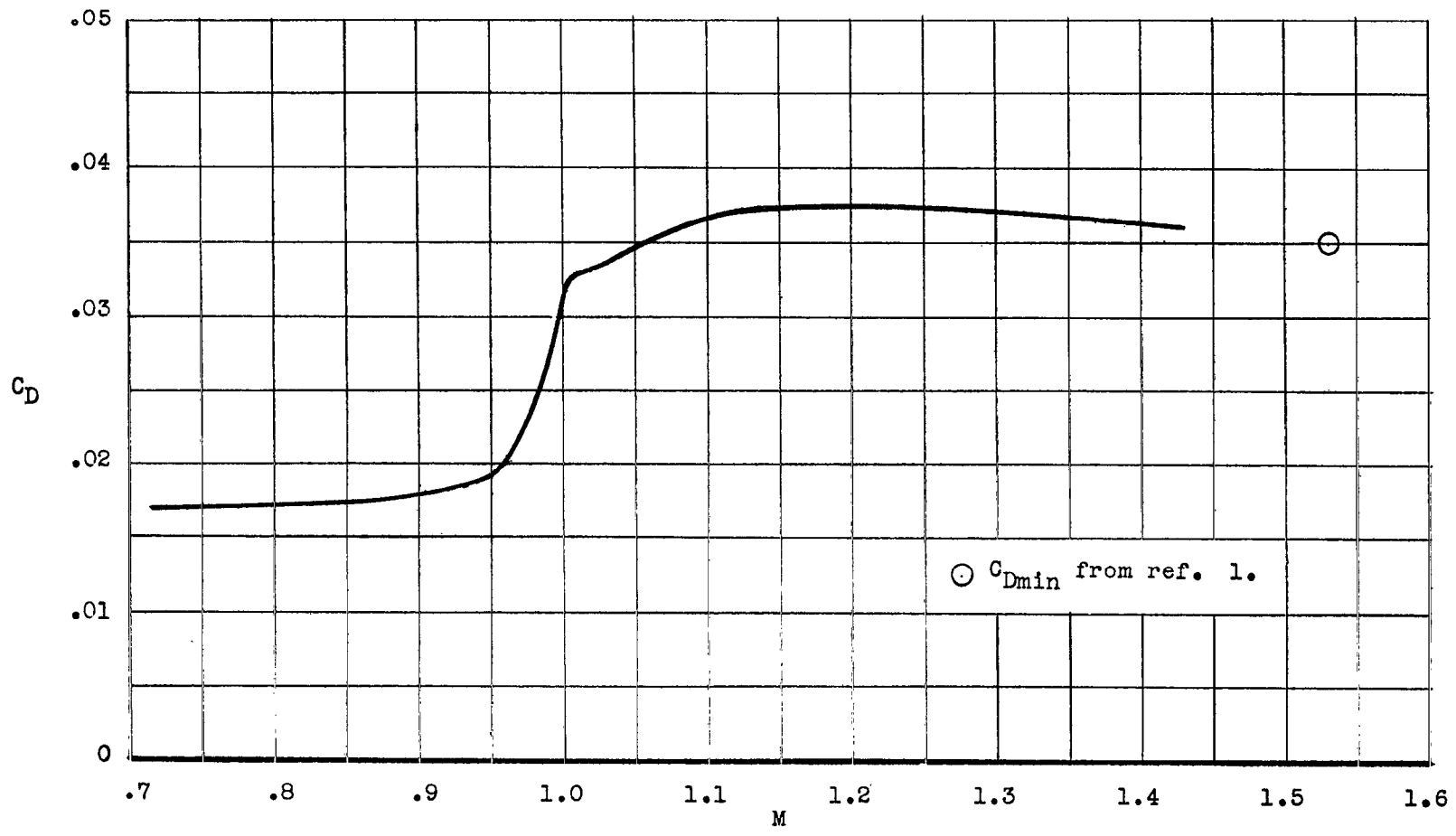


Figure 12.- The variation of the total drag coefficient with Mach number for the trim conditions of the test. Drag increment contributed by exit areas included.

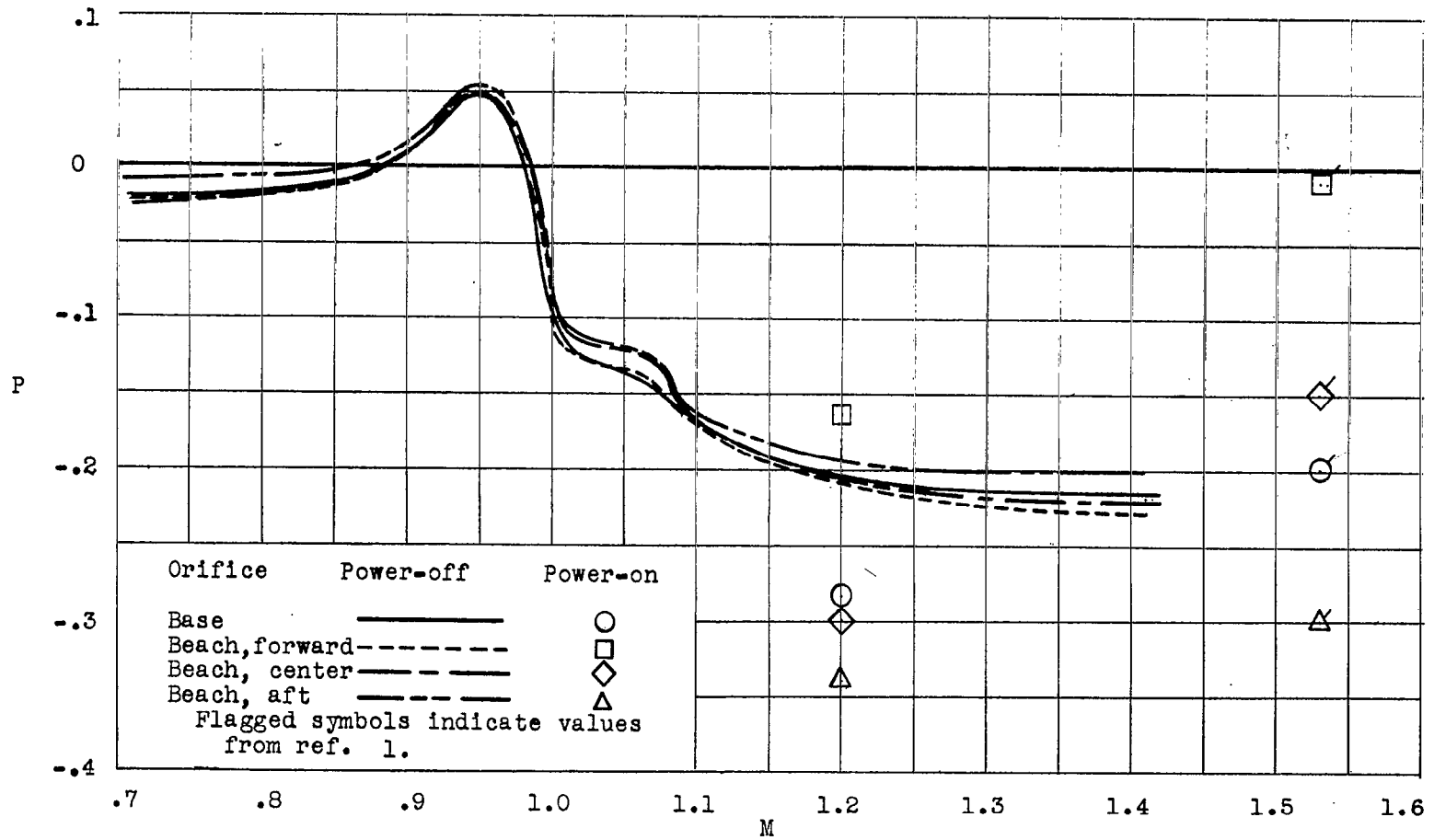


Figure 13.- Variations of pressure coefficients on base and beach with Mach number.

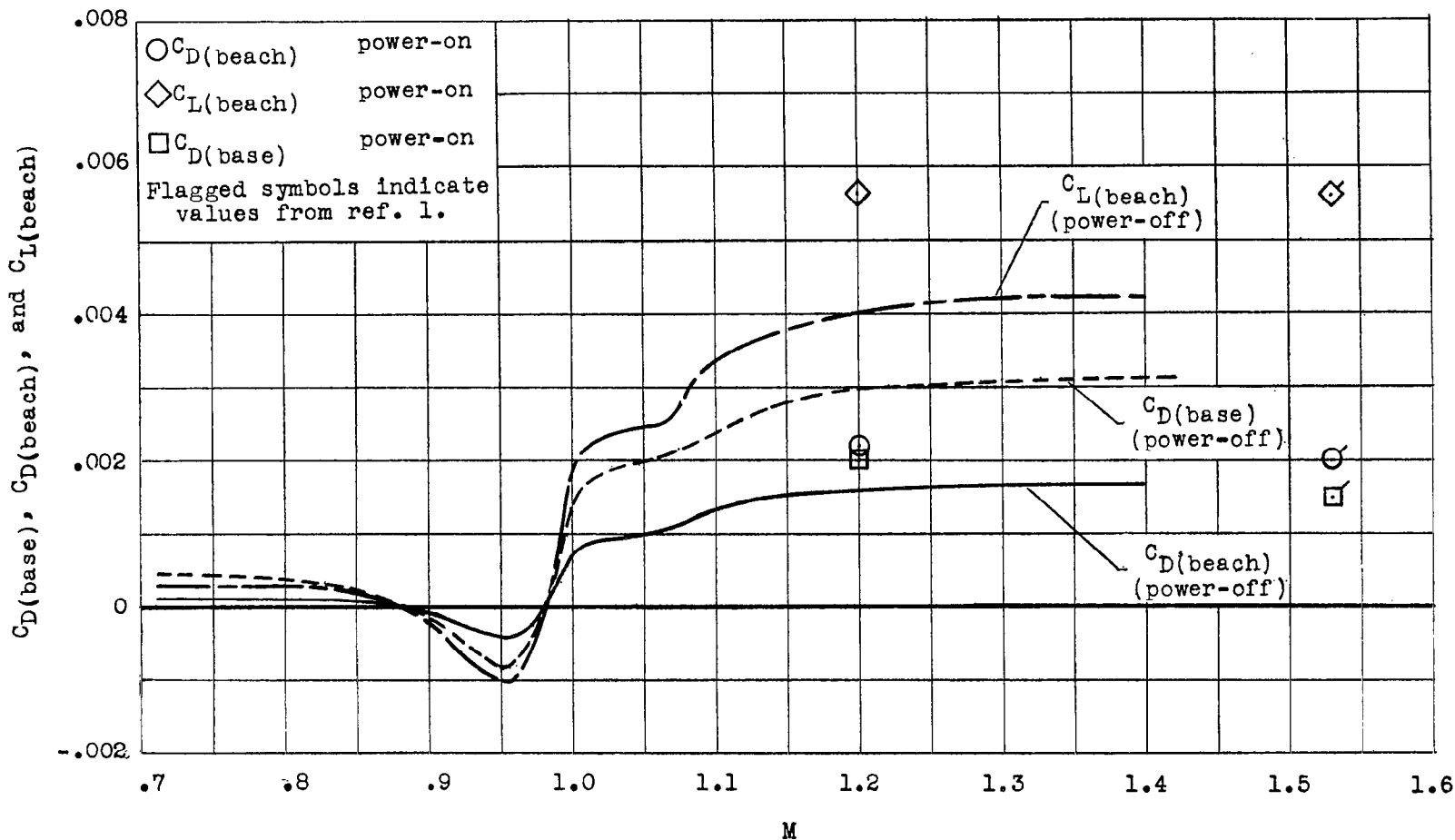


Figure 14.- Variations of the base-drag coefficient and the beach lift and drag coefficients with Mach number.

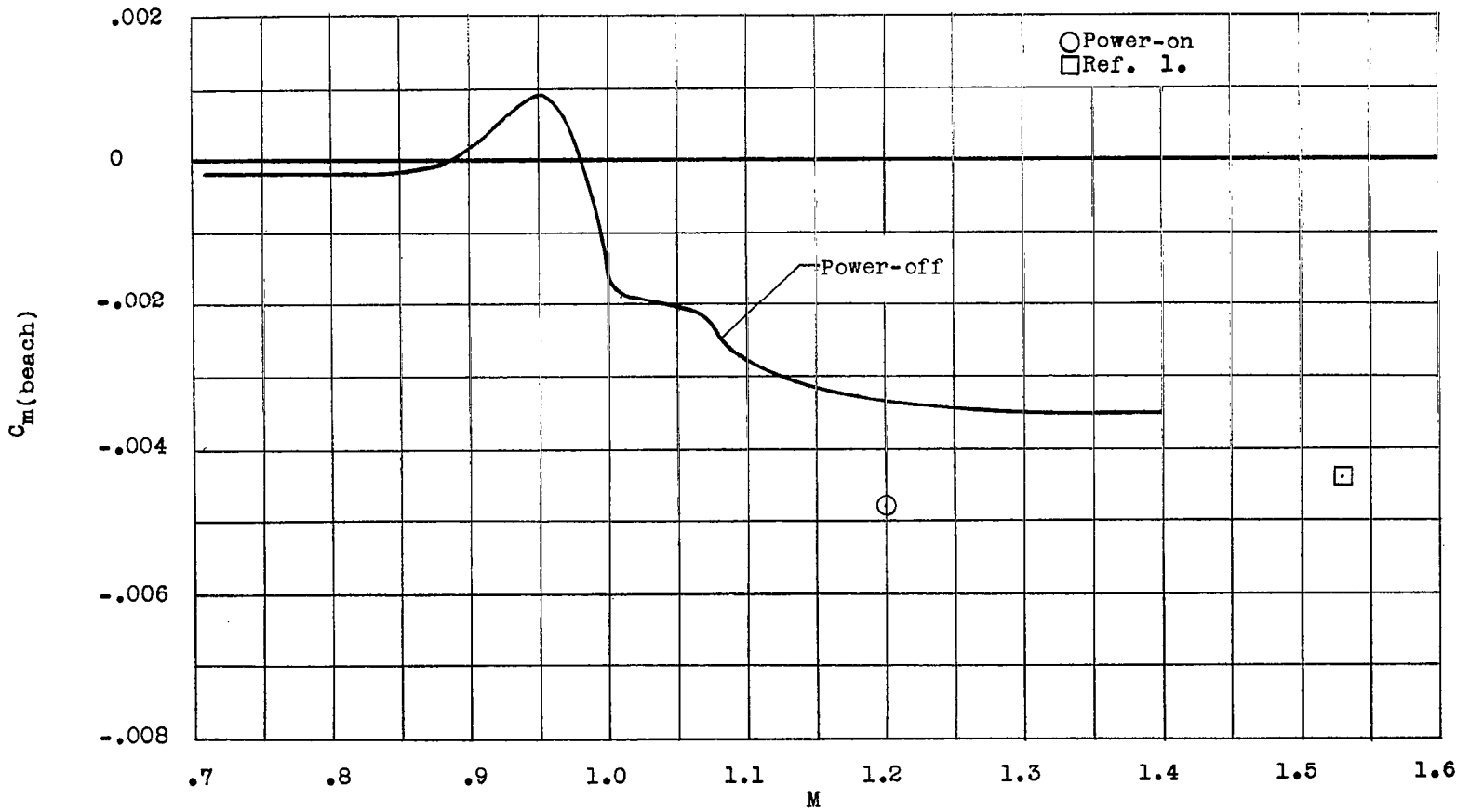


Figure 15.- Variation with Mach number of the beach pitching-moment coefficient.

NASA Technical Library



3 1176 01438 6750

CONFIDENTIAL